Solution of the EEG inverse problem by random dipole sampling

L. Della Cioppa[1*], M. Tartaglione[2*], A. Pascarella[3] and F. Pitolli[4]

[1]University of Roma "La Sapienza" and Istituto di Scienze Marine - CNR, Roma, Italy

E-mail: lorenzo.dellacioppa@artov.ismar.cnr.it

[2]University of Roma "La Sapienza", Roma, Italy

E-mail: michela.tartaglione@sbai.uniroma1.it

[3]Istituto per le Applicazioni del Calcolo "Mauro Picone" - CNR, Roma, Italy

E-mail: a.pascarella@iac.cnr.it

[4]University of Roma "La Sapienza", Roma, Italy

E-mail: francesca.pitolli@uniroma1.it

[*] These authors contributed equally to this work

November 2023

Abstract. Electroencephalography (EEG) source imaging aims to reconstruct brain activity maps from the neuroelectric potential difference measured on the skull. To obtain the brain activity map, we need to solve an ill-posed and ill-conditioned inverse problem that requires regularization techniques to make the solution viable. When dealing with real-time applications, dimensionality reduction techniques can be used to reduce the computational load required to evaluate the numerical solution of the EEG inverse problem. To this end, in this paper we use the random dipole sampling method, in which a Monte Carlo technique is used to reduce the number of neural sources. This is equivalent to reducing the number of the unknowns in the inverse problem and can be seen as a first regularization step. Then, we solve the reduced EEG inverse problem with two popular inversion methods, the weighted Minimum Norm Estimate (wMNE) and the standardized LOw Resolution brain Electromagnetic TomograAphy (sLORETA). The main result of this paper is the error estimates of the reconstructed activity map obtained with the randomized version of wMNE and sLORETA. Numerical experiments on synthetic EEG data demonstrate the effectiveness of the random dipole sampling method.

Keywords: EEG imaging, underdetermined inverse problem, random sampling, inversion method, wMNE, sLORETA

Submitted to: *Inverse Problems*

1. Introduction

The electroencephalography (EEG) inverse problem aims to reconstruct the neuroelectric activity map from the electric potential differences measured by a set of electrodes located on the skull. Since EEG is a non-invasive technique and EEG devices are quite cheap, EEG source imaging is widely used both in clinical applications and neuroscience studies. Furthermore, EEG measurements come to a high temporal resolution - on the order of milliseconds - making this brain imaging technique of primary interest in real-time applications. For details we refer the reader to [1, 2] and references therein.

What makes EEG source imaging tricky is the fact that to obtain the brain activity map, we have to solve a severely ill-posed inverse problem and regularization techniques are needed to make the solution viable [1,2]. Unfortunately, the numerical solution of the EEG inverse problem can be time and memory consuming, which makes it unattractive in real-time applications, especially when portable devices are employed. To reduce the computational cost, dimensionality reduction techniques can be used to extract the most significant features from the data or to select the brain regions of interest before applying an inversion method [3–5]. In addition, dimensionality reduction can act as a first regularization step, since it reduces the degrees of freedom of the inverse problem.

In this paper, we consider a slim dimensionality reduction technique - the random dipole sampling method - where the dimensionality reduction is achieved by using a Monte Carlo technique to reduce the number of the unknowns - neural sources - without imposing any a priori information. This method was introduced in [6] to solve the magnetoencephalography (MEG) inverse problem, in which neuroelectric activity maps are reconstructed from the neuromagnetic field measured outside the head [1,7]. Tests on synthetic and real magnetic data have shown that the method has a low computational load while keeping good accuracy [8,9]. Here, we use the random dipole sampling method for reducing the dimensionality of the EEG inverse problem and show its effectiveness when using weighted Minimum Norm Estimate (wMNE) [10] and standardized LOw Resolution brain Electromagnetic TomograAphy (sLORETA) [11] to reconstruct the brain activity map. The wMNE and sLORETA algorithms are two of the most popular inversion methods for EEG imaging and are also easy to implement. For this reason, they are particularly suitable for real-time applications. The main result of this paper is the error estimate for the reconstructed activity map obtained by the randomized version of wMNE and sLORETA. In the previous papers [6, 8, 9], the effectiveness of the method was shown through numerical tests but no error estimates were provided. The estimates we provide give an upper bound for the error and allow us to identify the optimal number of dipoles that need to be sampled to achieve good accuracy. Numerical experiments conducted on synthetic EEG data confirm our findings.

In literature, random methods are commonly used for dimensionality reduction of regression problems (see, for instance, [12–15]) while their use for the solution of inverse problems is still limited and mainly based on the randomized singular value

decomposition (randSVD) described in [16]. In [17–21] randSVD was used to solve inverse problems by classical regularization methods, i.e., Tikhonov regularization and truncated SVD. A different approach was proposed in [22], where the authors introduced a sampled iterative method that converges to the Tikhonov solution. A randomized method for MEG/EEG imaging was introduced in [23] with the aim of simultaneously detecting cortical and subcortical brain activity [24]. The method decomposes the source space into multiple randomized multiresolution levels, then solves the MEG/EEG inverse problem by a hierarchical Bayesian model implying Mimimum Norm Estimate (MNE) as a particular case.

The random dipole sampling method we consider was introduce in [6] and is related in some way to the random column sampling method described in [25], but its motivation stems from the neurophysiological assumption that brain activity is spatially sparse [26] and therefore only a small number of neural sources are sufficient to represent the neuroelectric current flowing in the brain. The key ingredient of the method is that the neural sources are chosen randomly by drawing from the uniform probability distribution, making the method easy to implement and efficient when dealing with real-time applications. Here, we use the method along with wMNE and sLORETA to solve the EEG inverse problem.

The paper is organized as follows. In Sect. 2 some preliminaries on linear algebra and the EEG inverse problem are given as well as the description of the random dipole sampling method. The main results of the paper are given in Sect. 3, where the error estimates are obtained. The results of the numerical experiments we conducted are displayed in Sect. 4, while a discussion of our findings is given in Sect. 5. Finally, in Sect. 6 we draw some conclusions and outline future developments.

2. Materials and Methods

In this section, after recalling some basic facts from linear algebra (see Sect. 2.1), we describe the EEG inverse problem and the inversion methods we are interested in (see Sect. 2.2). The random dipole sampling method is described in Sect. 2.3.

2.1. Linear algebra preliminaries

In this section we recall same definitions and properties that we will use in the following. For details, we refer to the classical books on linear algebra [27, 28] and the review paper [15].

Let $v = [v_1, \dots, v_n] \in \mathbb{R}^n$ be a real vector and $A = [a_{kj}, 1 \le k \le m, 1 \le j \le n] \in \mathbb{R}^{m\times n}$ be a real matrix. The symbol $\|v\|$ denotes the Euclidean norm of vectors while $\|A\|$ denotes the usual spectral norm of matrices. We write $\|A\|_F$ for the Frobenius norm. We recall that

$$\|A\| = \sigma_1(A), \qquad \|A\|_F = \Big(\sum_{i=1}^{r} \sigma_i(A)^2\Big)^{1/2}, \tag{2.1}$$

where $\sigma_1(A) \geq \sigma_2(A) \geq \cdots \geq \sigma_r(A)$ are the singular values of A and $r = rank(A)$. It follows that

$$\|A\| \leq \|A\|_F \leq \sqrt{r}\,\|A\|. \tag{2.2}$$

Both norms are unitarily invariant, i.e., for any matrix $A \in \mathbb{R}^{m\times n}$

$$\|UAV\| = \|A\|, \qquad \|UAV\|_F = \|A\|_F, \tag{2.3}$$

where $U \in \mathbb{R}^{m\times m}$ and $V \in \mathbb{R}^{n\times n}$ are orthonormal matrices.

The condition number of a matrix A is

$$\kappa(A) = \sigma_1(A)/\sigma_r(A). \tag{2.4}$$

We will make use of the following inequalities (see, [27]). For any rectangular matrices A, $\delta A \in \mathbb{R}^{m\times n}$ it holds

$$\sigma_{max}(A + \delta A) \leq \sigma_{max}(A) + \|\delta A\|, \tag{2.5}$$

$$\sigma_{min}(A + \delta A) \geq \sigma_{min}(A) - \|\delta A\|. \tag{2.6}$$

In the following we will also make use of the following property of norms. For any pair of vectors v and u and matrices A and B it holds

$$\Big|\|v\| - \|u\|\Big| \leq \|v - u\|, \qquad \Big|\|A\| - \|B\|\Big| \leq \|A - B\|. \tag{2.7}$$

2.2. The EEG inverse problem

The EEG inverse problem aims to reconstruct the neuroelectric current flowing inside the brain once the electric difference potential on the scalp, generated by the activity of one or more neuroelectric sources, is given. The cortical surfaces are extracted from MRI images and discretized in a regular triangulation whose nodes form the source space. A current dipole is located in each point $\mathbf{r}^k = [r_x^k, r_y^k, r_z^k]$, $1 \leq k \leq n$, of the source space. The unknown is the current dipole moment vector $Q = [\mathbf{q}^1, \ldots, \mathbf{q}^n]$, where $\mathbf{q}^k = [q_x^k, q_y^k, q_z^k]$ is the dipole moment of the k-th dipole.

We assume that the measurement vector $b \in \mathbb{R}^m$ and the current dipole moment vector $Q \in \mathbb{R}^{3n}$ are linearly related, i.e.,

$$b = M\,Q \tag{2.8}$$

where $M = [M(\mathbf{r}^1), \ldots, M(\mathbf{r}^n)] \in \mathbb{R}^{m\times 3n}$ is the lead field matrix. The sub-matrix $M(\mathbf{r}^k) \in \mathbb{R}^{m\times 3}$, $1 \leq k \leq n$, represents the electric potential produced by a unit current dipole located in $\mathbf{r}^k$. For details see [2, 7].

It is well known that the EEG inverse problem is an underdetermined ill-posed and ill-conditioned inverse problem [1, 2] for which regularization techniques are needed to obtain a feasible solution. Two of the most widely used inversion methods for solving the EEG inverse problem are the weighted Minimum Norm Estimate (wMNE) [29] and standardized LOw Resolution brain Electromagnetic TomogrAphy (sLORETA) [11] algorithms.

The estimated current distribution obtained by wMNE is

$$Q_{wMNE} = (M^T\Sigma^{-1}M + R^{-1})^{-1}M^T\Sigma^{-1}b, \tag{2.9}$$

where $R \in \mathbb{R}^{3n\times 3n}$ is the source covariance matrix and $\Sigma \in \mathbb{R}^{m\times m}$ is the noise covariance matrix. R is a diagonal matrix whose diagonal entries are

$$R_{jj} = \|M(\mathbf{r}^k)\|^{-\rho}, \quad 1+3(k-1) \le j \le 3k, \quad 1 \le k \le n, \tag{2.10}$$

where ρ is the depth weighting parameter. For the EEG inverse problem suitable values of ρ are in the interval $(0, 5]$, depending on the source density, the dipole orientation and the SNR [29].
Without loss of generality, we can assume the data has been whitened so that $\Sigma = I$. Thus, defining the inversion matrix

$$G_{wMNE} = M^TM + R^{-1}, \tag{2.11}$$

the wMNE solution can be written as

$$Q_{wMNE} = G^{-1}_{wMNE}M^Tb. \tag{2.12}$$

Starting from the estimate Q_{wMNE}, sLORETA produces a statistical measure of the brain activity normalizing the wMNE estimate w.r.t. the variance of the estimated sources. For any dipole, sLORETA produces a neural activity index z^k as follows,

$$z^k = (\mathbf{q}^k_{wMNE})^T(\Sigma^k_{Q_{wMNE}})^{-1}\mathbf{q}^k_{wMNE}, \tag{2.13}$$

where $\mathbf{q}^k_{wMNE}$ is the estimated activity of the dipole located in $\mathbf{r}^k$ and $\Sigma^k_{Q_{wMNE}} \in \mathbb{R}^{3\times 3}$ is the k-th diagonal block of the variance of the estimated sources $\Sigma_{Q_{wMNE}} \in \mathbb{R}^{3n\times 3n}$. It can be shown that

$$\Sigma_{Q_{wMNE}} = (M^TM + R^{-1})^{-1}M^TM = G^{-1}_{wMNE}M^TM, \tag{2.14}$$

usually known as the wMNE resolution matrix.

When the cortical surface is known, the dipoles have fixed orientations since they are perpendicular to the cortical surface. In this case, the unknowns are the intensity of the n sources, i.e., $Q = [\|\mathbf{q}^1\|, \ldots, \|\mathbf{q}^n\|]$, and the orientations can be plugged into the lead field M, which now is an $m \times n$ matrix. Similarly to (2.12), the wMNE solution $Q_{wMNE} = [\|\mathbf{q}^1_{wMNE}\|, \ldots, \|\mathbf{q}^n_{wMNE}\|]$ is given by [30]

$$Q_{wMNE} = G^{-1}_{wMNE}M^Tb, \tag{2.15}$$

where

$$G_{wMNE} = M^TM + R^{-1} \in \mathbb{R}^{n\times n}, \tag{2.16}$$

and $R \in \mathbb{R}^{n\times n}$ has diagonal entries

$$R_{kk} = \|M(\mathbf{r}^k)\|^{-\rho}, \quad 1 \le k \le n, \tag{2.17}$$

being $M(\mathbf{r}^k)$ a vector.
In case of fixed orientation, the sLORETA index simplifies as

$$z^k = \frac{\|\mathbf{q}^k_{wMNE}\|^2}{\Sigma^k_{Q_{wMNE}}}, \qquad 1 \le k \le n, \tag{2.18}$$

where $\Sigma^k_{Q_{wMNE}}$ is the k-th entry of the $n \times n$ source covariance matrix $\Sigma_{Q_{wMNE}}$. It can be shown [31] that (2.18) is equivalent to

$$z^k = \frac{\|\mathbf{q}^k_{wMNE}\|^2}{\|(R(\mathbf{r}^k))^T(M(\mathbf{r}^k))^T(MRM^T + I)^{-1}M(\mathbf{r}^k)R(\mathbf{r}^k)\|^2_F}, \ 1 \leq k \leq n. \quad (2.19)$$

2.3. Random dipole sampling method

We can use the random sampling to select a small subset of source points so reducing the number of columns of the lead field matrix. Let $\mathcal{I}_c = (k_1, \ldots, k_c)$ denote a subset of c indices of the dipoles drawn from the uniform probability distribution with replacement. We will denote by ν_k, $k \in \mathcal{I}_c$, with $c \geq \nu_k \geq 1$, the number of times the k-th dipole was drawn. The sampled lead field matrix is

$$M_S = \sqrt{\frac{n}{c}} MS \in \mathbb{R}^{m \times 3c}, \quad (2.20)$$

where the entries of the sampling matrix $S \in \mathbb{R}^{3n \times 3c}$ are all zeros except for the 3×3 blocks

$$S^{kj} = (S_{s,t}, 1 + 3(k-1) \leq s \leq 3k, 1 + 3(j-1) \leq t \leq 3j) = I_3, \quad k \in \mathcal{I}_c, \quad 1 \leq j \leq c,$$

indicating that the k-th source point was drawn at the j-th drawing. Assuming $c \ll n$, the sampled lead field matrix M_S has far fewer columns than the full matrix M. The factor $\sqrt{\frac{n}{c}}$ ensures that the singular values of M_S are an unbiased estimate of the singular values of M [15].

We can obtain an approximate solution of the EEG inverse problem by using M_S in either wMNE or sLORETA. Thus, the estimated randomized neuroelectric current

$$\widetilde{Q}_{wMNE} = [\tilde{\mathbf{q}}^{k_1}_{wMNE}, \ldots, \tilde{\mathbf{q}}^{k_c}_{wMNE}],$$

obtained using wMNE as inverse solver, is given by

$$\widetilde{Q}_{wMNE} = \widetilde{G}^{-1}_{wMNE} M_S^T b, \qquad \widetilde{G}_{wMNE} = M_S^T M_S + R_S^{-1} \in \mathbb{R}^{3c \times 3c}, \quad (2.21)$$

where $R_S \in \mathbb{R}^{3c \times 3c}$ can be obtained from R retaining just the entries corresponding to the drawn dipoles. Since R is a diagonal matrix, it follows that

$$R_S^{-1} = \frac{n}{c} S^T R^{-1} S. \quad (2.22)$$

Similarly, the randomized sLORETA statistical measure is

$$\tilde{z}^k = (\tilde{\mathbf{q}}^k_{wMNE})^T (\tilde{\Sigma}^k_{\tilde{Q}_{wMNE}})^{-1} \tilde{\mathbf{q}}^k_{wMNE}, \qquad k \in \mathcal{I}_c, \quad (2.23)$$

where $\tilde{\Sigma}^k_{\tilde{Q}_{wMNE}}$ is the variance of the estimated sources $\tilde{Q}_{wMNE}$.

In case of fixed orientation, the randomized wMNE method estimates the intensity vector $\tilde{Q}_{wMNE} = [\|\tilde{\mathbf{q}}^{k_1}_{wMNE}\|, \ldots, \|\tilde{\mathbf{q}}^{k_c}_{wMNE}\|]$ so that the sampled lead field matrix is

$$M_S = \sqrt{\frac{n}{c}} MS \in \mathbb{R}^{m \times c}, \quad (2.24)$$

where the only entries of the sampling matrix $S \in \mathbb{R}^{n\times c}$ different from zeros are the entries (k, j), $k \in \mathcal{I}_c$, $1 \le j \le c$, which are equal to 1.
In this case, the randomized wMNE solution is given by

$$\widetilde{Q}_{wMNE} = \widetilde{G}^{-1}_{wMNE} M_S^T b, \tag{2.25}$$

with

$$\widetilde{G}_{wMNE} = M_S^T M_S + R_S^{-1} \in \mathbb{R}^{c\times c}, \quad R_S \in \mathbb{R}^{c\times c}, \tag{2.26}$$

while the randomized sLORETA index becomes

$$\widetilde{z}^k = \frac{\|\tilde{\mathbf{q}}^k_{wMNE}\|^2}{\|(R(\mathbf{r}^k))^T (M(\mathbf{r}^k))^T (M_S R_S M_S^T + I)^{-1} M(\mathbf{r}^k) R(\mathbf{r}^k)\|_F^2}, \quad k \in \mathcal{I}_c. \tag{2.27}$$

3. Error estimates

In this section we define the local reconstruction error for the randomized version of both wMNE and sLORETA and obtain deterministic estimates for these errors. We note that in order for the estimates of Theorems 3.3 and 3.6 to hold with high probability, we can repeat the random dipole sampling algorithm a suitable number of times [16].
For the sake of simplicity, in the following we consider the case of fixed orientation. The results can be easily extended to the general case (see Section 4.2).

3.1. Randomized wMNE

For the randomized wMNE method we define the local reconstruction error as

$$\mathcal{E}^k_{wMNE} = \begin{cases} \left| \|\mathbf{q}^k_{wMNE}\| - \|\widetilde{\mathbf{q}}^k_{wMNE}\| \right|, & \text{if} \quad k \in \mathcal{I}_c, \\ \|\mathbf{q}^k_{wMNE}, \| & \text{if} \quad k \notin \mathcal{I}_c. \end{cases} \tag{3.1}$$

We note that

$$S^T Q_{wMNE} = [\|\mathbf{q}^{k_1}_{wMNE}\|, \ldots, \|\mathbf{q}^{k_c}_{wMNE}\|].$$

In the following we will denote by $\bar{S}$ the matrix that selects the dipoles that have not been drawn, i.e., $\bar{S}^T Q_{wMNE} = [\|\mathbf{q}^k_{wMNE}\|, k \notin \mathcal{I}_c]$. It is easy to show that $\|S^T\| = (\max\limits_{k\in\mathcal{I}_c} \nu_k)^{1/2}$ while $\|\bar{S}^T\| = 1$. Moreover, we define the sampling identity matrix $I_S = SS^T \in \mathbb{R}^{n\times n}$. I_S is a diagonal matrix whose only entries different from zero are the diagonal entries having indices $k \in \mathcal{I}_c$. These entries are equal to ν_k.

Proposition 3.1. *Let G_{wMNE} and $\widetilde{G}_{wMNE}$ be the full and the sampled inversion matrices, respectively. For the minimum singular value of G_{wMNE} and $\widetilde{G}_{wMNE}$ the following bounds hold*

$$\sigma_{min}(G_{wMNE}) \ge \mu, \qquad \sigma_{min}(\widetilde{G}_{wMNE}) \ge \mu, \tag{3.2}$$

where $\mu = \max_{1\le k\le n} \|M(\mathbf{r}^k)\|^{\rho/2}$.

The proof is in the appendix.

Proposition 3.2. *Let Q_{wMNE} and $\widetilde{Q}_{wMNE}$ be the neuroelectric current estimates obtained with the exact wMNE and the randomized wMNE, respectively. The following estimates hold*

$$\|S^T Q_{wMNE} - \widetilde{Q}_{wMNE}\| \leq \max(\frac{n}{c}\nu - 1, 1)\sqrt{\nu}\frac{\kappa(G_{wMNE})}{\sigma_{min}(\widetilde{G}_{wMNE})}\|M^T b\|, \quad (3.3)$$

where $\nu = \max\limits_{1\leq k\leq c} \nu_k \geq 1$, and

$$\|\bar{S}^T Q_{wMNE}\| \leq \frac{1}{\sigma_{min}(G_{wMNE})}\|M^T b\|. \quad (3.4)$$

The proof is in the appendix.

Theorem 3.3. *For the reconstruction error $\mathcal{E}_{wMNE}$ the following estimate holds*

$$\mathcal{E}^k_{wMNE} \leq \begin{cases} \max(\frac{n}{c}\nu - 1, 1)\sqrt{\nu}\,\frac{\kappa(G_{wMNE})}{\mu}\|M^T b\|, & \text{if } \; k \in \mathcal{I}_c, \\ \\ \frac{1}{\mu}\|M^T b\|, & \text{if } \; k \notin \mathcal{I}_c, \end{cases} \quad (3.5)$$

where $\mu = \max_{1\leq k\leq n} \|M(\mathbf{r}^k)\|^{\rho/2}$.

Proof. Since $\left|\|\mathbf{q}^k_{wMNE}\| - \|\widetilde{\mathbf{q}}^k_{wMNE}\|\right| \leq \|S^T Q_{wMNE} - \widetilde{Q}_{wMNE}\|$, $k \in \mathcal{I}_c$, and $\|\mathbf{q}^k_{wMNE}\| \leq \|S^T_N Q_{wMNE}\|$ the claim follows combining Propositions 3.1-3.2. □

Since $\sqrt{\nu}(\frac{n}{c}\nu - 1)\frac{\kappa(G_{wMNE})}{\mu}\|M^T b\| \geq \frac{1}{\mu}\|M^T b\|$, we can obtain a bound for the error vector $\mathcal{E}_{wMNE} = [\mathcal{E}^1_{wMNE}, \ldots, \mathcal{E}^n_{wMNE}]$, i.e.,

$$\|\mathcal{E}_{wMNE}\| \leq \max(\frac{n}{c}\nu - 1, 1)\sqrt{\nu}\,\frac{\kappa(G_{wMNE})}{\mu}\|M^T b\|.$$

From (2.15) it follows $M^T b = G_{wMNE} Q_{wMNE}$. Thus, we obtain the following bound for the relative error,

$$\frac{\|\mathcal{E}_{wMNE}\|}{\|Q_{wMNE}\|} \leq \max(\frac{n}{c}\nu - 1, 1)\sqrt{\nu}\,\frac{\kappa(G_{wMNE})\sigma_{max}(G_{wMNE})}{\mu}. \quad (3.6)$$

Remark 1. In case of uniform sampling without replacement we have $\|S^T\| = 1$ and $\|I - \frac{n}{c}I_S\| \leq \|I - \frac{n}{c}I_S\|_F = \sqrt{2(n-c)}$ so that the estimate in (3.3) becomes

$$\|S^T Q_{wMNE} - \widetilde{Q}_{wMNE}\| \leq \sqrt{2(n-c)}\,\frac{\kappa(G_{wMNE})}{\sigma_{min}(\widetilde{G}_{wMNE})}\|M^T b\|.$$

Moreover, $\|\bar{S}^T Q_{wMNE}\| \to 0$ when $c \to n$. Thus, as expected, in this case the reconstruction error $\mathcal{E}_{wMNE}$ goes to 0 when $c \to n$.

Remark 2. In case of Tikhonov regularization the solution can be written as

$$Q_{Tik} = (M^T M + \alpha I)^{-1} M^T b, \quad (3.7)$$

where $\alpha > 0$ is the regularization parameter. Q_{Tik} is also known as minimum norm estimate. Its random version is

$$\tilde{Q}_{Tik} = (M_S^T M_S + \alpha I)^{-1} M_S^T b. \tag{3.8}$$

Thus, the error estimate in Theorem 3.3 can be easily adapted to the randomized Tikhonov method by substituting in (3.5) μ with α and $\kappa(G_{wMNE})$ with $\kappa(M^T M + \alpha I)$. Furthermore, we can obtain the error estimate for the randomized least squares solution

$$\tilde{Q}_{LSQ} = (M_S^T M_S)^{-1} M_S^T b, \tag{3.9}$$

by substituting μ with $\sigma_{min}(M^T M)$ and $\kappa(G_{wMNE})$ with $\kappa(M^T M)$.

3.2. Randomized sLORETA

In this section we give an upper bound for the reconstruction error when using randomized sLORETA to solve the EEG inverse problem. Recalling (2.19) and (2.27), we define the local error as

$$\mathcal{E}_{sL}^k = \left| \sqrt{z^k} - \sqrt{\tilde{z}^k} \right| = \begin{cases} \left| \dfrac{\|\mathbf{q}_{wMNE}^k\|}{\|L(\mathbf{r}^k)\|_F} - \dfrac{\|\tilde{\mathbf{q}}_{wMNE}^k\|}{\|L_S(\mathbf{r}^k)\|_F} \right|, & \text{if} \quad k \in \mathcal{I}_c, \\ \dfrac{\|\mathbf{q}_{wMNE}^k\|}{\|L(\mathbf{r}^k)\|_F}, & \text{if} \quad k \notin \mathcal{I}_c, \end{cases} \tag{3.10}$$

where

$$L(\mathbf{r}^k) = (R(\mathbf{r}^k))^T (M(\mathbf{r}^k))^T (MRM^T + I)^{-1} M(\mathbf{r}^k) R(\mathbf{r}^k), \ 1 \le k \le n, \tag{3.11}$$

and

$$L_S(\mathbf{r}^k) = (R(\mathbf{r}^k))^T (M(\mathbf{r}^k))^T (M_S R_S M_S^T + I)^{-1} M(\mathbf{r}^k) R(\mathbf{r}^k), \ k \in \mathcal{I}_c. \tag{3.12}$$

We note that $L(\mathbf{r}^k), L_S(\mathbf{r}^k) \in \mathbb{R}^{3\times 3}$.

Lemma 3.4. *For the difference of the reciprocals of $\|L(\mathbf{r}^k)\|_F$ and $\|L_S(\mathbf{r}^k)\|_F$ the following bound holds*

$$\left| \frac{1}{\|L(\mathbf{r}^k)\|_F} - \frac{1}{\|L_S(\mathbf{r}^k)\|_F} \right| \le \frac{2}{\xi}, \tag{3.13}$$

where $\xi = \min_{1\le k\le n} \sigma_{min}(L(\mathbf{r}^k))$.

The proof is in the appendix.

Proposition 3.5. *Let $\widetilde{Q}_{wMNE}$ be the neuroelectric current estimate obtained with the randomized wMNE. It holds*

$$\|\widetilde{Q}_{wMNE}\| \le \frac{1}{\mu} \|M^T b\|, \qquad \|Q_{wMNE}\| \le \frac{1}{\mu} \|M^T b\|, \tag{3.14}$$

where $\mu = \max_{1\le k\le n} \|M(\mathbf{r}^k)\|^{\rho/2}$.

The proof is in the appendix.

Theorem 3.6. *For the local reconstruction error $\mathcal{E}_{sL}$ the following estimate holds*

$$\mathcal{E}_{sL}^k \leq \begin{cases} \dfrac{1}{\mu\xi}\left(\max(\dfrac{n}{c}\nu - 1, 1)\sqrt{\nu}\,\kappa(G_{wMNE}) + 2\right)\|M^T b\|, & \text{if } \ k \in \mathcal{I}_c, \\ \dfrac{1}{\mu\xi}\|M^T b\|, & \text{if } \ k \notin \mathcal{I}_c, \end{cases} \tag{3.15}$$

where $\mu = \max_{1\leq k\leq n}\|M(\mathbf{r}^k)\|^{\rho/2}$ and $\xi = \min_{1\leq k\leq n}\sigma_{min}(L(\mathbf{r}^k))$.

Proof. When $k \in \mathcal{I}_c$ we have

$$\begin{aligned} \left|\frac{\|\mathbf{q}_{wMNE}^k\|}{\|L(\mathbf{r}^k)\|_F} - \frac{\|\tilde{\mathbf{q}}_{wMNE}^k\|}{\|L_S(\mathbf{r}^k)\|_F}\right| \ &\leq \ \left|\|\mathbf{q}_{wMNE}^k\| - \|\tilde{\mathbf{q}}_{wMNE}^k\|\right| \frac{1}{\|L(\mathbf{r}^k)\|_F} \\ &+ \ \left|\frac{1}{\|L(\mathbf{r}^k)\|_F} - \frac{1}{\|L_S(\mathbf{r}^k)\|_F}\right| \|\tilde{\mathbf{q}}_{wMNE}^k\|. \end{aligned}$$

The first term in the r.h.s. is related to the wMNE reconstruction error while the second term is related to the error produced by the sampling procedure applied to the lead field matrix.
From (2.7) it follows $\left|\|\mathbf{q}_{wMNE}^k\| - \|\tilde{\mathbf{q}}_{wMNE}^k\|\right| \leq \|\mathbf{q}_{wMNE}^k - \tilde{\mathbf{q}}_{wMNE}^k\|$. Thus, we can use the results in Theorem 3.3 to bound the first term.
As for the second term, since $\|\tilde{\mathbf{q}}_{wMNE}^k\| \leq \|\widetilde{Q}_{wMNE}\|$, combining Lemma 3.4 and Proposition 3.5 we get

$$\left|\frac{1}{\|L(\mathbf{r}^k)\|_F} - \frac{1}{\|L_S(\mathbf{r}^k)\|_F}\right| \|\tilde{\mathbf{q}}_{wMNE}^k\| \leq \frac{2}{\xi}\frac{1}{\mu}\|M^T b\|.$$

When $k \notin \mathcal{I}_c$, the bound easily follows recalling that $\|\mathbf{q}_{wMNE}^k\| \leq \|Q_{wMNE}\|$, and combining Lemma 3.4 and Proposition 3.2.

□

4. Results

To show the effectiveness of randomized wMNE and randomized sLORETA methods we conducted some numerical experiments on synthetic EEG data. The latter have been generated by solving the forward EEG problem in OpenMEEG software [32] using a source space obtained by an average subject [33] containing 25000 points and an EEG helmet with 65 sensors at an average distance of 10 cm from the origin of the head coordinate system. One single dipole was randomly selected from the source space and activated by a unitary current dipole moment with fixed orientation. The measurement vector b was then obtained by applying (2.8) and by adding Gaussian noise with SNR = 10dB and SNR = 20dB. A coarser source space containing 15000 points was used to solve the inverse problem, that is the lead field matrix is $M \in \mathbb{R}^{m\times n}$, with $n = 15000$ and $m = 65$. The inverse problem was solved by wMNE and sLORETA methods implemented in Brainstorm software [34]. To improve the accuracy, the inverse problem was solved $N = 10$ times, each time using a different sampling matrix. In our

α	$\kappa(G_{wMNE})$	ξ
1/10	1662.02	4.46
1/9	1346.43	4.56
1/8	1064.05	4.69
1/7	814.90	4.86
1/6	598.97	5.10
1/5	416.25	5.44
1/4	266.76	5.97
1/3	150.49	6.55
1/2	67.44	7.761
1	17.61	11.63
2	5.15	19.62
3	2.85	27.71
4	2.04	35.84
5	1.66	44.01

Table 1. Condition number $\kappa(G_{wMNE})$ and the quantity ξ (see Lemma 3.4) for different values of the regularization parameter α.

experiments, no significant improvement has been observed by increasing N.
In Section 4.1, we present a comprehensive set of numerical tests in the case of fixed orientation. In Section 4.2, we present some numerical tests for the free orientation case.

4.1. Fixed orientation

Since the error estimates $\mathcal{E}_{wMNE}$ and $\mathcal{E}_{sL}$ depend on the condition number $\kappa(G_{wMNE})$ and on the quantities ξ and μ (see Theorems 3.3 and 3.6), first of all we computed their values for different values of the regularization parameter α. We note that in Brainstorm the regularization parameter is included in the matrix R; the default value is $\alpha = 3$. The computed values of $\kappa(G_{wMNE})$ and ξ are listed in Table 1. As expected, the condition number $\kappa(G_{wMNE})$ approaches 1 while the regularization parameter increases. Conversely, ξ decreases. Thus, the error estimates $\mathcal{E}_{wMNE}$ and $\mathcal{E}_{sL}$ decrease for increasing α. Table 2 shows how μ (see Proposition 3.1) changes with respect to the depth weighting parameter ρ. We note that the default in Brainstorm is ρ between 0 and 1. As expected, the values follow an exponential growth.

Then, we studied how the reconstruction errors $\mathcal{E}_{wMNE}$ and $\mathcal{E}_{sL}$, as defined in (3.6) and (3.10), depend on the number of sampled columns c. The numerical experiments have been carried out for different values of c, ranging from a minimum of $c = 500$ columns to a maximum of $c = 15000$ columns. In this test we used the default values for α and ρ. The averaged absolute errors $\|\mathcal{E}_{wMNE}\|$ and $\|\mathcal{E}_{sL}\|$ are shown in Figure 1 while the relative error $\frac{\|\mathcal{E}_{wMNE}\|}{\|Q_{wMNE}\|}$ is shown in Figure 2. To reduce the computational cost of the dipole sampling method, we sampled the columns with replacement. For

ρ	μ
0.10	1.41
0.25	2.38
0.50	5.68
0.75	13.54
1	32.28

Table 2. The quantity μ (see Proposition 3.1) for different values of the depth weighting parameter ρ.

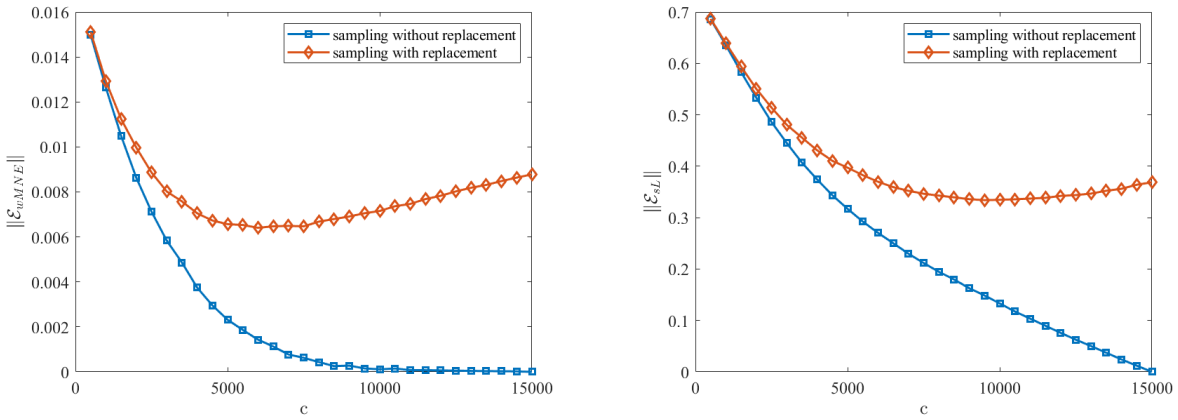

Figure 1. (a) The absolute error $\|\mathcal{E}_{wMNE}\|$ versus the number of sampled columns c, in the case of sampling with replacement and sampling without replacement. (b) The absolute error $\|\mathcal{E}_{sL}\|$ versus the number of sampled columns c, in the case of sampling with replacement and sampling without replacement.

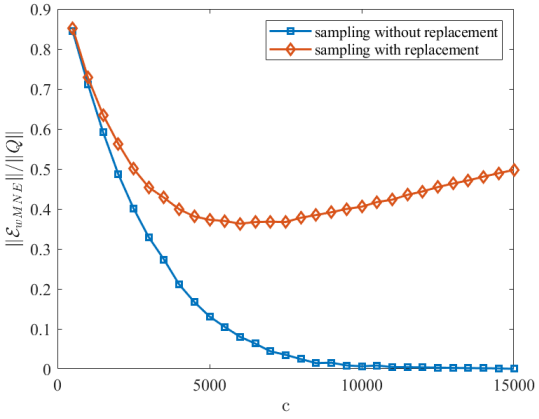

Figure 2. The relative error $\frac{\|\mathcal{E}_{wMNE}\|}{\|Q_{wMNE}\|}$ versus the number of sampled columns c, in the case of sampling with replacement and sampling without replacement.

Table 3. The average DLE and the standard deviation σ (mm) for $n = 15000$ and different source depth (LOC = S (superficial sources at least 50 mm from the origin of the head coordinate system), M (middle sources between 30 and 50 mm from the origin of the head coordinate system), D (deep sources at less then 30 mm from the origin of the head coordinate system))

SNR	LOC	inversion method	$c = 100$ DLE (σ)	$c = 500$ DLE (σ)	$c = 1000$ DLE (σ)	$c = 2000$ DLE (σ)	full DLE (σ)
10	S	sLORETA	16.6 (7.2)	13.3 (6.8)	12.5 (5.4)	10.9 (5.2)	13.9 (5.3)
10	S	wMNE	14.5 (5.6)	17.2 (8.6)	17.7 (8.8)	18.8 (9.6)	16.6 (7.6)
10	M	sLORETA	15.8 (7.5)	11.7 (4.7)	11.5 (5.8)	10.2 (5.5)	12.6 (5.9)
10	M	wMNE	21.9 (7.5)	27.6 (9.0)	28.4 (9.3)	28.0 (9.5)	25.5 (8.2)
10	D	sLORETA	18.2 (5.5)	11.6 (4.6)	9.5 (4.3)	9.0 (4.3)	15.2 (4.4)
10	D	wMNE	23.7 (8.3)	28.8 (8.1)	31.3 (9.1)	32.4 (9.4)	29.0 (8.9)
20	S	sLORETA	16.4 (6.6)	12.0 (5.3)	11.1 (5.0)	10.4 (4.9)	12.9 (4.8)
20	S	wMNE	14.6 (5.8)	17.1 (7.9)	17.9 (8.2)	18.1 (8.0)	16.2 (6.9)
20	M	sLORETA	15.5 (7.3)	10.6 (5.2)	9.6 (5.2)	8.8 (4.4)	11.7 (5.9)
20	M	wMNE	21.0 (7.2)	25.4 (6.9)	26.6 (7.7)	26.2 (7.9)	22.7 (5.8)
20	D	sLORETA	17.6 (5.4)	11.2 (3.9)	8.8 (3.3)	8.0 (3.6)	15.0 (3.6)
20	D	wMNE	22.8 (7.3)	26.0 (6.1)	27.5 (7.4)	29.2 (7.6)	26.0 (6.1)

comparison, we evaluated the errors also in case of sampling without replacement.

Finally, since our aim is to show that the random sampling method is efficient in localizing neural sources, we evaluated the distance localization error (DLE), i.e., the distance between the real source and the center of mass of the reconstructed current distribution. The DLE is a common metric used in the MEG/EEG community to test the accuracy of the reconstructed neural current [35]. For the random dipole sampling method, we compute the center of mass of the source localizations obtained in 10 different runs of the method. The number of sampled columns c ranges from 100 to 2000 and the results are averaged over 1000 simulations. Figure 3 shows the boxplots for superficial, middle and deep sources when SNR=10dB and SNR=20dB while the average DLE and the standard deviation are listed in Table 3. For comparison, the results obtained using the full source space are also shown.

To analyze the effect of the source space size, we performed numerical tests for $n = 2000, 4000, 8000$. Figures 4–5 show the boxplots of DLE across 100 simulations for superficial, middle and deep sources when SNR=10dB and SNR=20dB. The average DLE and the standard deviation are listed in Tables 4–6.

In Figure 6 the median of the condition number $\kappa(G_{wMNE})$ across 100 simulations for different values of the number of sampled columns c is plotted.

Table 4. The average DLE and the standard deviation σ (mm) for $n = 2000$ and different source depth (LOC = S (superficial sources at least 50 mm from the origin of the head coordinate system), M (middle sources between 30 and 50 mm from the origin of the head coordinate system), D (deep sources at less then 30 mm from the origin of the head coordinate system))

SNR	LOC	inversion method	$c = 100$ DLE (σ)	$c = 500$ DLE (σ)	$c = 1000$ DLE (σ)	full DLE (σ)
10	S	sLORETA	17.3 (6.2)	13.5 (5.5)	13.1 (5.5)	14.4 (4.3)
10	S	wMNE	17.0 (7.8)	18.3 (8.8)	19.1 (9.5)	19.1 (10.0)
10	M	sLORETA	16.3 (6.4)	12.9 (6.2)	12.7 (7.3)	13.7 (6.3)
10	M	wMNE	22.0 (9.7)	25.4 (9.6)	25.8 (11.1)	24.1 (11.4)
10	D	sLORETA	16.5 (6.9)	11.9 (5.0)	12.1 (6.2)	14.0 (5.5)
10	D	wMNE	23.7 (9.8)	26.6 (10.6)	27.1 (9.5)	28.1 (11.4)
20	S	sLORETA	16.4 (6.0)	12.5 (4.8)	12.2 (4.6)	13.7 (4.3)
20	S	wMNE	16.0 (6.6)	17.0 (7.3)	16.4 (7.6)	16.7 (7.2)
20	M	sLORETA	15.2 (6.5)	11.1 (5.3)	10.8 (5.5)	12.6 (5.9)
20	M	wMNE	19.2 (7.0)	21.8 (7.4)	22.8 (7.8)	19.4 (7.8)
20	D	sLORETA	15.1 (6.3)	10.7 (4.3)	9.9 (4.8)	13.1 (5.1)
20	D	wMNE	21.2 (9.6)	24.3 (8.8)	24.1 (7.5)	25.6 (11.0)

Table 5. The average DLE and the standard deviation σ (mm) for $n = 4000$ and different source depth (LOC = S (superficial sources at least 50 mm from the origin of the head coordinate system), M (middle sources between 30 and 50 mm from the origin of the head coordinate system), D (deep sources at less then 30 mm from the origin of the head coordinate system))

SNR	LOC	inversion method	$c = 100$ DLE (σ)	$c = 500$ DLE (σ)	$c = 1000$ DLE (σ)	$c = 2000$ DLE (σ)	full DLE (σ)
10	S	sLORETA	17.2 (6.2)	12.8 (5.9)	11.9 (5.9)	10.7 (5.6)	18.8 (7.1)
10	S	wMNE	16.3 (6.8)	20.2 (10.6)	21.9 (13.3)	29.8 (23.6)	98.1 (26.9)
10	M	sLORETA	15.2 (6.6)	12.1 (5.4)	11.2 (5.4)	11.2 (5.6)	24.8 (9.2)
10	M	wMNE	21.1 (7.2)	27.0 (10.8)	35.6 (14.3)	49.4 (21.9)	57.5 (23.6)
10	D	sLORETA	15.0 (6.3)	12.8 (6.3)	11.8 (5.6)	12.4 (5.4)	30.5 (7.5)
10	D	wMNE	24.7 (9.7)	31.7 (12.7)	41.3 (14.8)	54.6 (18.8)	52.4 (19.0)
20	S	sLORETA	15.4 (6.5)	11.4 (5.2)	10.2 (4.5)	9.5 (4.6)	18.3 (6.5)
20	S	wMNE	14.9 (6.0)	18.3 (9.0)	19.7 (11.7)	29.2 (23.6)	97.5 (26.9)
20	M	sLORETA	14.3 (6.7)	10.7 (4.2)	10.0 (4.6)	9.7 (5.0)	23.0 (8.0)
20	M	wMNE	19.3 (7.1)	24.3 (9.3)	33.8 (12.2)	49.4 (22.6)	58.2 (23.8)
20	D	sLORETA	14.4 (6.4)	11.3 (5.1)	10.3 (4.4)	10.9 (5.0)	29.1 (7.0)
20	D	wMNE	22.9 (7.9)	28.9 (10.0)	38.4 (15.8)	54.4 (20.3)	52.1 (18.6)

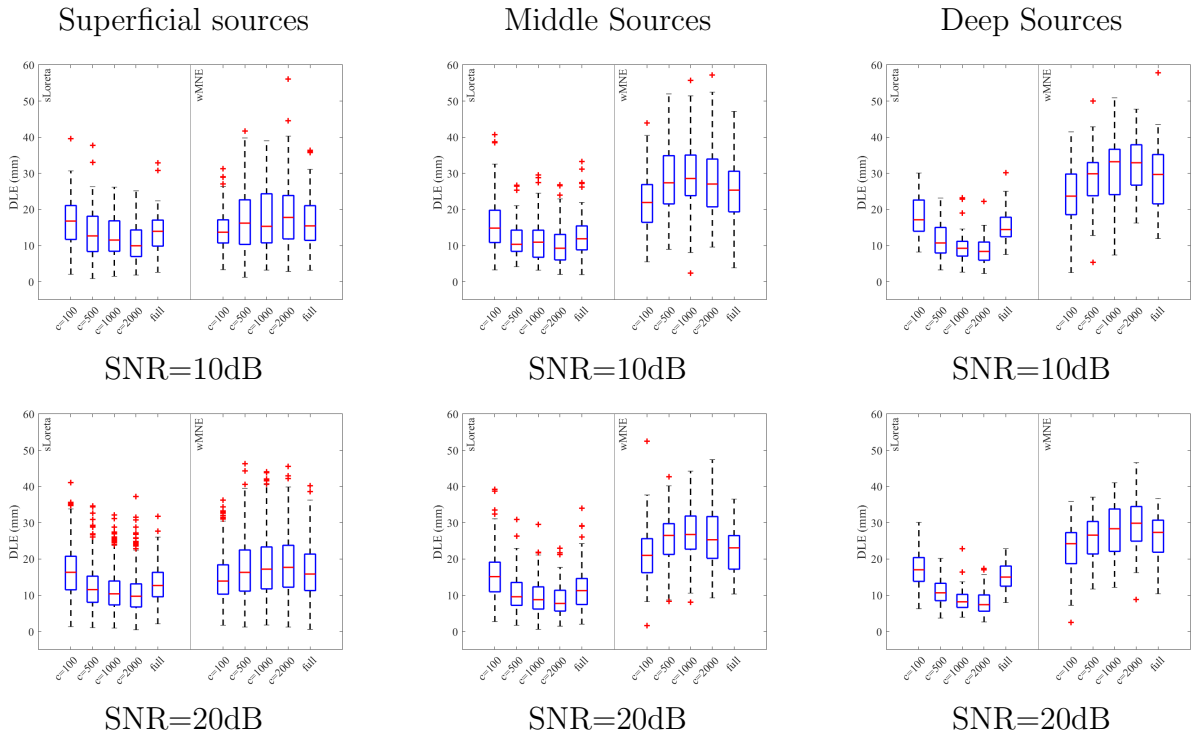

Figure 3. Boxplots of DLE across 100 simulations for $n = 15000$ when SNR=10dB (first row) and SNR = 20dB (second row). First column refers to superficial sources (at least 50 mm from the origin of the head coordinate system), second column refers to middle sources (between 30 and 50 mm from the origin of the head coordinate system), third column refers to deep sources (at less then 30 mm from the origin of the head coordinate system).

4.2. Free orientation

In case of free orientation we define the local reconstruction error for wMNE as

$$\mathcal{E}^k_{wMNE} = \begin{cases} \|\mathbf{q}^k_{wMNE} - \widetilde{\mathbf{q}}^k_{wMNE}\|, & \text{if} \quad k \in \mathcal{I}_c, \\ \|\mathbf{q}^k_{wMNE}\|, & \text{if} \quad k \notin \mathcal{I}_c. \end{cases} \tag{4.1}$$

Since $\|\mathbf{q}^k_{wMNE} - \widetilde{\mathbf{q}}^k_{wMNE}\| \leq \|S^T Q_{wMNE} - \widetilde{Q}_{wMNE}\|$, $k \in \mathcal{I}_c$, and $\|\mathbf{q}^k_{wMNE}\| \leq \|S^T_N Q_{wMNE}\|$, the estimate in Theorem 3.3 holds also in this case.
For sLORETA the local reconstruction error is defined as

$$\mathcal{E}^k_{sL} = \begin{cases} \left|z^k - \tilde{z}^k\right|, & \text{if} \quad k \in \mathcal{I}_c, \\ \left|z^k\right|, & \text{if} \quad k \notin \mathcal{I}_c, \end{cases} \tag{4.2}$$

where z^k and $\tilde{z}^k$ are given in (2.13) and (2.23), respectively. It can be shown that

$$\begin{aligned} |z^k - \tilde{z}^k| \quad &\leq \quad (\|\mathbf{q}^k_{wMNE}\| \, \|(\Sigma^k_{Q_{wMNE}})^{-1}\| + \|\tilde{\mathbf{q}}^k_{wMNE}\| \, \|(\tilde{\Sigma}^k_{Q_{wMNE}})^{-1}\|)\mathcal{E}^k_{wMNE} \\ &+ \quad \|\mathbf{q}^k_{wMNE}\| \cdot \|\tilde{\mathbf{q}}^k_{wMNE}\| \cdot \|(\Sigma^k_{Q_{wMNE}})^{-1} - (\tilde{\Sigma}^k_{Q_{wMNE}})^{-1}\| \end{aligned} \tag{4.3}$$

The first term depends on the wMNE local reconstruction error while the second term is related to the error of the covariance matrix. Since $\|\mathbf{q}^k_{wMNE}\| \leq \|Q_{wMNE}\|$ and

Table 6. The average DLE and the standard deviation σ (mm) for $n = 8000$ and different source depth (LOC = S (superficial sources at least 50 mm from the origin of the head coordinate system), M (middle sources between 30 and 50 mm from the origin of the head coordinate system), D (deep sources at less then 30 mm from the origin of the head coordinate system))

SNR	LOC	inversion method	$c = 100$ DLE (σ)	$c = 500$ DLE (σ)	$c = 1000$ DLE (σ)	$c = 2000$ DLE (σ)	full DLE (σ)
10	S	sLORETA	16.1 (5.9)	11.9 (5.2)	10.6 (5.1)	9.8 (4.4)	19.4 (8.4)
10	S	wMNE	15.9 (6.4)	19.5 (9.3)	21.3 (9.5)	22.5 (12.6)	96.2 (33.2)
10	M	sLORETA	14.9 (7.1)	11.5 (5.5)	11.3 (5.0)	9.5 (4.8)	27.3 (8.7)
10	M	wMNE	20.2 (7.8)	28.4 (9.6)	30.1 (11.9)	36.7 (14.4)	68.8 (26.9)
10	D	sLORETA	14.0 (6.0)	11.2 (4.6)	10.6 (4.5)	10.5 (4.5)	32.1 (6.6)
10	D	wMNE	23.4 (8.6)	30.7 (12.6)	36.5 (11.9)	42.9 (16.9)	69.3 (27.3)
20	S	sLORETA	15.0 (5.9)	10.7 (4.4)	9.2 (4.2)	8.6 (4.0)	18.8 (8.2)
20	S	wMNE	14.6 (5.6)	18.4 (9.0)	19.5 (8.0)	21.2 (13.0)	96.5 (32.2)
20	M	sLORETA	13.4 (6.6)	10.2 (4.7)	8.9 (4.0)	7.2 (3.3)	26.2 (8.3)
20	M	wMNE	19.3 (6.5)	24.0 (8.0)	26.6 (10.7)	36.0 (15.6)	67.9 (25.2)
20	D	sLORETA	13.8 (5.3)	10.0 (4.4)	9.6 (4.1)	8.3 (3.6)	31.1 (5.8)
20	D	wMNE	20.8 (8.0)	27.9 (9.3)	33.1 (10.5)	41.4 (17.0)	69.1 (27.0)

$\|\tilde{\mathbf{q}}^k_{wMNE}\| \leq \|\tilde{Q}_{wMNE}\|$, estimates in Proposition 3.5 holds. Moreover,

$$\|(\Sigma^k_{Q_{wMNE}})^{-1} - (\tilde{\Sigma}^k_{Q_{wMNE}})^{-1}\| \leq \frac{1}{\sigma_{min}(\Sigma^k_{Q_{wMNE}})} + \frac{1}{\sigma_{min}(\tilde{\Sigma}^k_{Q_{wMNE}})}. \quad (4.4)$$

Using estimates (3.14) and (4.4) in (4.3), we obtain the upper bound for the local sLORETA error

$$|z^k - \tilde{z}^k| \leq \frac{2}{\mu\,\xi}\|M^T b\|\Big(\mathcal{E}^k_{wMNE} + \frac{1}{\mu}\|M^T b\|\Big), \quad (4.5)$$

where $\xi = \min(\sigma_{min}(\Sigma^k_{Q_{wMNE}}), \sigma_{min}(\tilde{\Sigma}^k_{Q_{wMNE}}))$. Thus, the sLORETA local error behaves as the wMNE local error.

To show the effectiveness of the random dipole sampling method even in the free orientation case, we performed numerical tests with $n = 15000$ and SNR = 20dB. The boxplots of the DLE in Figure 7 show that the DLE is comparable to that obtained in the fixed orientation case.

5. Discussion

5.1. Related methods

Monte Carlo methods have a long history dating back to the middle of the twentieth century [36]. Since then, these methods have been widely used in scientific computing, for instance for integrating differential equations or probability distributions. In numerical linear algebra randomness is commonly used to initialize iterative methods

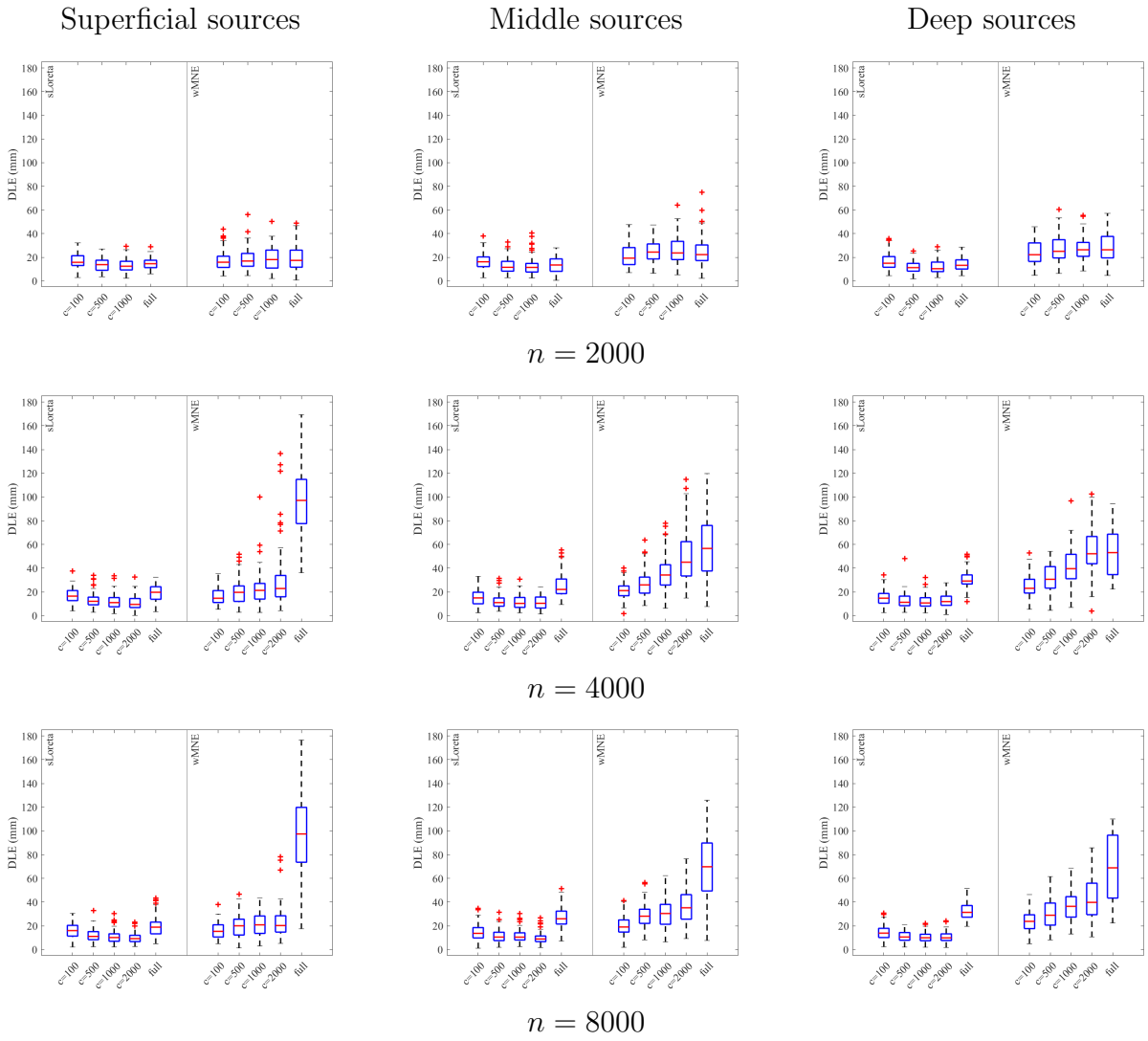

Figure 4. Boxplots of DLE across 1000 simulations when SNR=10dB for $n = 2000$ (first row), $n = 4000$ (second row), $n = 8000$ (third row). First column refers to superficial sources (at least 50 mm from the origin of the head coordinate system), second column refers to middle sources (between 30 and 50 mm from the origin of the head coordinate system), third column refers to deep sources (at less then 30 mm from the origin of the head coordinate system).

[28]. The first papers in which randomized methods were used to construct low-rank approximations of matrices are from the late 1990s [37, 38]. Nowadays, these methods are successfully used in several fields, such as computer science, numerical linear algebra, regression problems. For a comprehensive review on randomized methods we refer the reader to [15, 16].

There are many ways randomness comes into play in the solution of the MEG/EEG inverse problem. In the Bayesian framework Markov Chain Monte Carlo methods are usually used to sample posterior densities (see [3, 39] and references therein). In parametric methods the number of sources is modeled as a random variable while

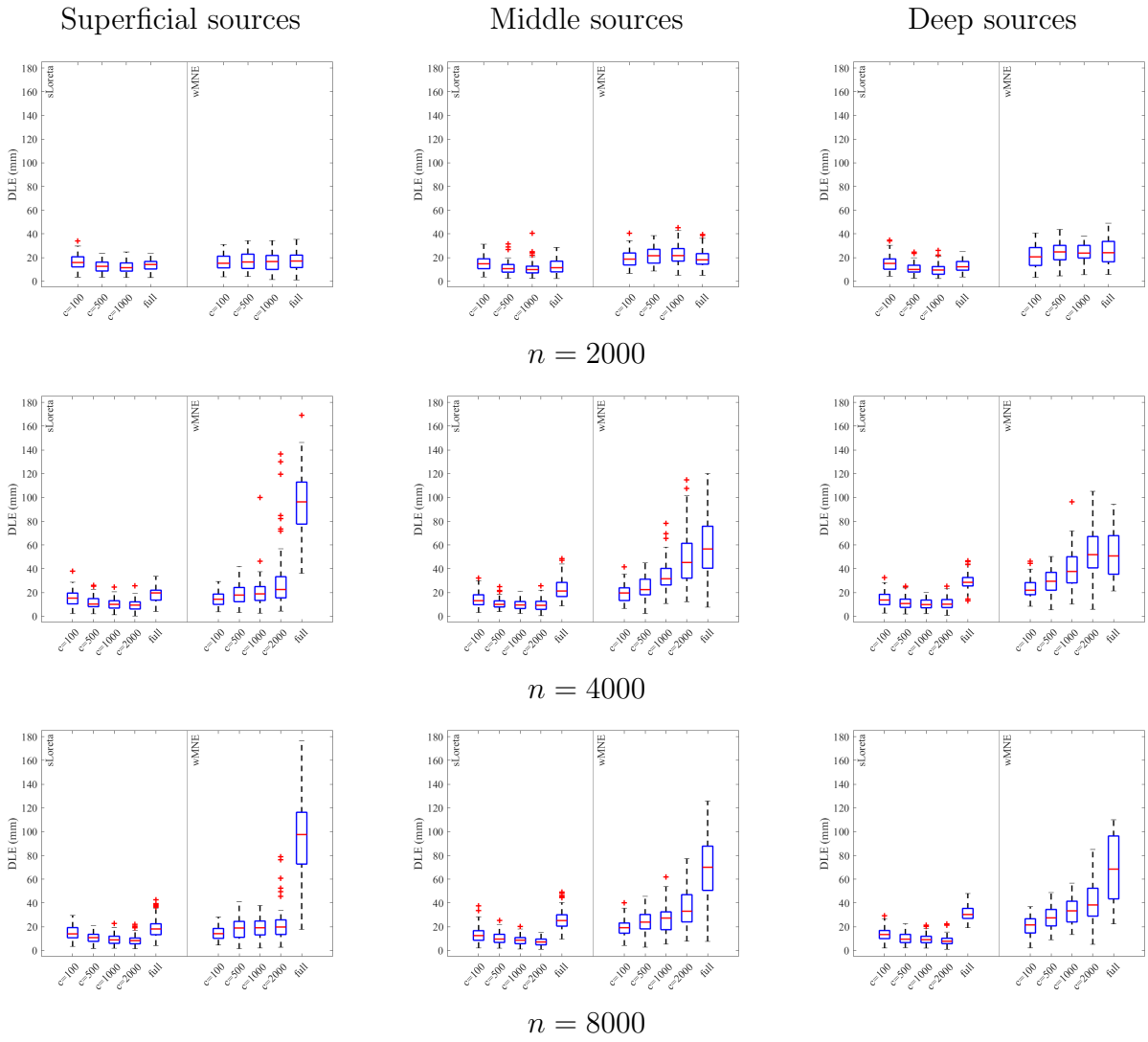

Figure 5. Boxplots of DLE across 100 simulations when SNR=20dB for $n = 2000$ (first row), $n = 4000$ (second row), $n = 8000$ (third row). First column refers to superficial sources (at least 50 mm from the origin of the head coordinate system), second column refers to middle sources (between 30 and 50 mm from the origin of the head coordinate system), third column refers to deep sources (at less then 30 mm from the origin of the head coordinate system).

their locations and orientations are modeled as random vectors (see [31] and references therein). In the randomized multiresolution scanning method [23, 24] randomness is used to generate multiple randomized decompositions of the source space at different resolution levels.

The random dipole sampling method described in Section 2.3 uses a different strategy. It samples a small set of dipoles in the source space using the uniform probability distribution. Then, it solves an inverse problem where the unknowns are the dipole moments on the drawn (fixed) locations. The rationale behind the method is that we can assume the neuroelectric current $\mathbf{J}(\mathbf{r})$ to be spatially sparse so that it can

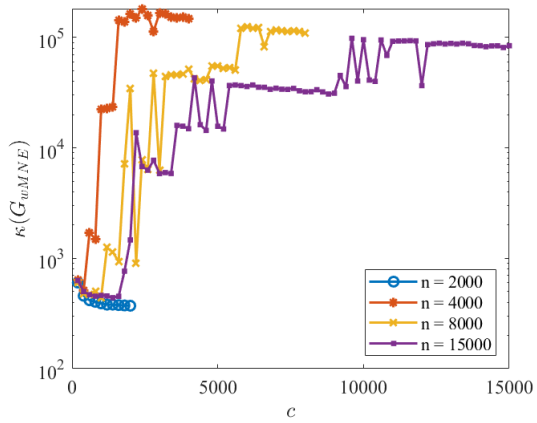

Figure 6. The median of the condition number $\kappa(G_{wMNE})$ across 100 simulations versus the number of sampled columns c for different values of n.

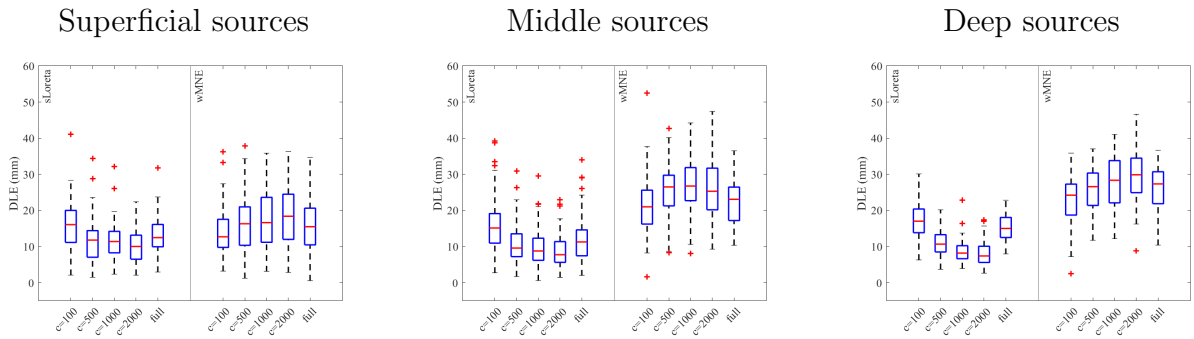

Figure 7. Boxplots of DLE across 100 simulations with $n = 15000$ and SNR=20dB in the free orientation case for superficial (a), middle (b), and deep (c) sources.

be represented using just few sources [40, 41], i.e.,

$$\mathbf{J}(\mathbf{r}) \approx \sum_{k \in \mathcal{I}_c} \mathbf{q}^k \, \delta(\mathbf{r} - \mathbf{r}^k).$$

The uniform distribution is a good choice when no prior information on the spatial distribution of the neuroelectric current is available. On the other hand, using different probability distributions would increase the computational cost.

Now, sampling c dipoles means to sample $3c$ columns in the lead field matrix since we select only the c sub-matrices $M(\mathbf{r}^k)$ corresponding to the dipoles with indices $k \in \mathcal{I}_c$. Thus, the random dipole sampling can be seen as a randomized column sampling procedure and it reduces to the column sampling introduced in [25, 42] in case of fixed orientation. For a given matrix $A \in \mathbb{R}^{m \times n}$ the column sampling is optimal when the columns are sampled using the probability distribution

$$p_k = \frac{\|A^{(k)}\|^2}{\sum_{k=1}^{n} \|A^{(k)}\|^2}, \qquad 1 \leq k \leq n,$$

where $A^{(k)}$ denotes the k-th column of A [15]. This is the same as dividing each column of the matrix A by p_k and then sampling the columns using the uniform distribution. We note that usually in wMNE the columns of the lead field matrix are normalized by a depth weighting that is related to the norm of the columns. This is evident when writing the wMNE solution (2.12) in the equivalent form [2]

$$Q_{wMNE} = RM^T(MRM^T + I)^{-1}b,$$

and justifies the use of the uniform distribution in the random dipole sampling method described in Section 2.3.

5.2. Our findings

As shown in Figures 1-2, the error with replacement and without replacement are comparable for lower values of c and the difference only gets relevant if $c > 5000$. In fact, in case of sampling without replacement the error goes to zero as the number of sampled columns approaches the maximum number of columns n, while in case of sampling with replacement the error decreases to a minimum located around $c = 6000$ for wMNE and $c = 9000$ for sLORETA. For higher values of c it grows slightly. This does not pose a strict restriction on the use of the random dipole sampling method, especially in real-time applications, as this method is aimed to significantly reduce the dimensionality of the EEG inverse problem, thus the goal is to use it for $c \leq 2000$.
The behavior of the error (see Figures 1–2) is in agreement with the estimates given in Section 3. In fact, when the number of sampled columns c is much smaller than n, due to factor $\max(\frac{n}{c}\nu - 1, 1)$ the error decreases rapidly as c increases reaching a minimum approximately for $\frac{n}{c}\nu = 2$. Then, the error increases slowly, roughly as ν. Instead, in case of sampling without replacement the error decreases monotonically as c increases and is equal to zero for $c = n$.
The numerical tests show that the choice $500 \leq c \leq 2000$ is a good compromise between accuracy and computational cost. This is more evident looking at the results shown in Figures 3–5 and Tables 3–6. When $n = 15000$ the DLE obtained by the random dipole sampling method with $c = 500, 1000, 2000$ is comparable to the error obtained using the full source space and is quite often even lower (see Figure 3 and Table 3). In general, sLORETA performs better than wMNE, regardless of source depth, in agreement with known results in the literature [43]. This is true for both SNR=10dB and SNR=20dB, causing the higher noise a slightly larger error, but still comparable with that of the full source space case. We note that even in the case of a smaller source space, the DLE values for the two noise levels are comparable.
When the size of the source space is reduced (see Figures 4–5 and Tables 4–6 where $n = 2000, 4000, 8000$) the DLE for sLORETA is lower when the number of sampled columns is $c = 2000$, i.e., c is in the order of n. The DLE for wMNE is lower both when $n = 2000$, for all values of c and even in case of full source space, and when $c = 100$, for all values of n. This means that wMNE is able to localize sources well not only when

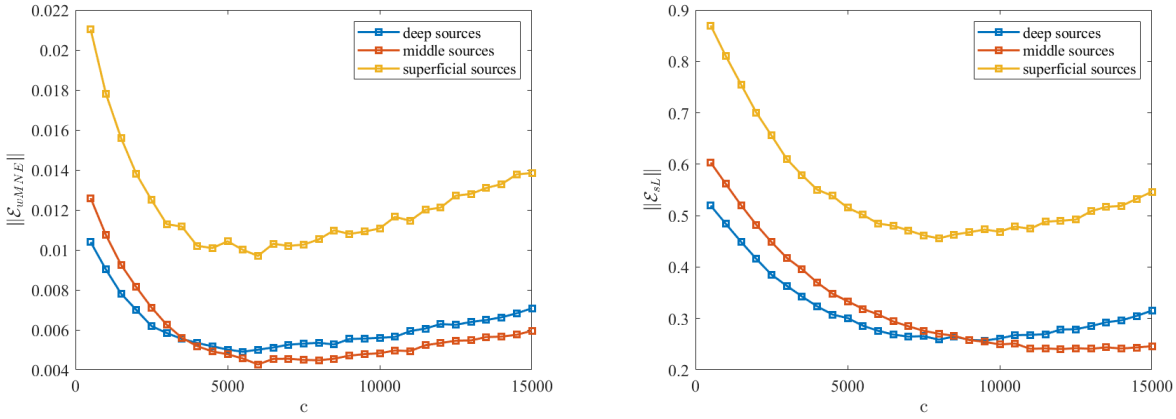

Figure 8. The averaged absolute error $\|\mathcal{E}_{wMNE}\|$ for wMNE (a) and sLORETA (b) versus the number of sampled columns c, in the case of sampling with replacement for superficial sources, middle sources and deep sources.

the source space has a low dimension, but also when few sources of a large source space are sampled by the random dipole sampling method. It is known that a low-dimensional source space can improve the localization of sparse neural sources [44] but this comes at the expense of low resolution. The random dipole sampling method has the same effect, with the advantage that the resolution can be easily improved by averaging the results obtained using different sampled source spaces. Interestingly, the reconstruction error is lower especially for deep and middle sources, as shown in Figure 8, where the norm of the local reconstruction error, averaged for different source depths, is displayed for both wMNE and sLORETA. This suggests that the sparsity induced by the random dipole sampling method is more effective for deep sources, according to the results in the literature (see, [24, 44]).

Finally, we note that the behavior of the localization error can be related to the conditioning of the matrix G_{wMNE}. In fact, the values of $\kappa(G_{wMNE})$ displayed in Figure 6 show that the condition number increases when c increases, being smaller when $n = 2000$ or when $c \leq 2000$.

6. Conclusion

In this paper, we analyzed in detail how to apply the random dipole sampling method for solving the inverse EEG problem. To the best of our knowledge, this is the first time that the random dipole sampling method has been used along with wMNE and sLORETA, two inversion methods well-known in the literature. The numerical tests have shown that the localization of neural sources produced by randomized wMNE and randomized sLORETA is comparable to that obtained when using the full source space. This suggests that the randomized version of wMNE and sLORETA can be successfully used in real-time applications, possibly with wearable systems, for which it is important

to reduce the computational cost of the inversion step.
To this end, it is important to analyze the performance of the random dipole sampling method in solving the inverse EEG problem in case of real data. In addition, the reconstruction error estimates we provided are deterministic. It would be interesting to obtain probabilistic error estimates. These topics will be the subject of future work.

7. Acknowledgment

The authors declare no conflicts of interest.
This research was partially funded by Gruppo Nazionale per il Calcolo Scientifico (Istituto Nazionale di Alta Matematica 'Francesco Severi'), grant INdAM–GNCS Project 2020 "Costruzione di metodi numerico/statistici basati su tecniche multiscala per il trattamento di segnali e immagini ad alta dimensionalità".

Appendix

Proof of Proposition 3.1

Using (2.16)-(2.17) and recalling that G_{wMNE} is the sum of two definite positive matrices we get

$$\sigma_{min}(G_{wMNE}) = \sigma_{min}(M^TM + R^{-1}) \geq \sigma_{min}(R^{-1}) = \max_{1\leq k\leq n} \|M(\mathbf{r}^k)\|^{\rho/2}.$$

The bound for $\sigma_{min}(\widetilde{G}_{wMNE})$ can be proved in a similar way.

Proof of Proposition 3.2

From (2.22),(2.26) and (2.24) it follows

$$\widetilde{G}_{wMNE} = M_S^T M_S + R_S^{-1} = \frac{n}{c} S^T (M^TM + R^{-1})S = \frac{n}{c} S^T G_{wMNE} S.$$

Hence, we get

$$\begin{aligned} S^TQ_{wMNE} - \widetilde{Q}_{wMNE} &= (S^TG_{wMNE}^{-1} - \widetilde{G}_{wMNE}^{-1}S^T)M^Tb \\ &= \widetilde{G}_{wMNE}^{-1}(\widetilde{G}_{wMNE}S^T - S^TG_{wMNE})G_{wMNE}^{-1}M^Tb \\ &= \widetilde{G}_{wMNE}^{-1}S^TG_{wMNE}(\tfrac{n}{c}I_S - I)G_{wMNE}^{-1}M^Tb. \end{aligned}$$

Taking the norm of both the l.h.s. and the last equality we obtain

$$\begin{aligned} \|S^TQ_{wMNE} - \widetilde{Q}_{wMNE}\| &= \widetilde{\|}G_{wMNE}^{-1}S^TG_{wMNE}(\tfrac{n}{c}I_S - I)G_{wMNE}^{-1}M^Tb\| \\ &\leq \|\widetilde{G}_{wMNE}^{-1}\|\|S^T\|\|G_{wMNE}\|\|I - \tfrac{n}{c}I_S\|\|G_{wMNE}^{-1}\|\|M^Tb\| \\ &\leq \frac{\kappa(G_{wMNE})}{\sigma_{min}(\widetilde{G}_{wMNE})}\|S^T\|\|I - \frac{n}{c}I_S\|\|M^Tb\|. \end{aligned}$$

Since $I - \frac{n}{c} I_S$ is a diagonal matrix whose entries corresponding to the indices $k \in \mathcal{I}_c$ are $1 - \frac{n}{c}\nu_k$, while the entries corresponding to the indices $k \notin \mathcal{I}_c$ are equal to 1, $\|I - \frac{n}{c} I_S\| = \max(\frac{n}{c}(\max_{k \in \mathcal{I}_c} \nu_k) - 1, 1)$ and the first estimate follows.
As for the second estimate, we have

$$\begin{aligned} \|\bar{S}^T Q_{wMNE}\| &= \|\bar{S}^T G_{wMNE}^{-1} M^T b\| \leq \\ &\leq \|G_{wMNE}^{-1}\| \|M^T b\| = \frac{1}{\sigma_{min}(G_{wMNE})} \|M^T b\|. \end{aligned}$$

Proof of Lemma 3.4

Using (2.2) and (2.6) we get

$$\begin{aligned} \left| \frac{1}{\|L(\mathbf{r}^k)\|_F} - \frac{1}{\|L_S(\mathbf{r}^k)\|_F} \right| &\leq \frac{1}{\|L(\mathbf{r}^k)\|_F} + \frac{1}{\|L_S(\mathbf{r}^k)\|_F} \\ &\leq \frac{1}{\sigma_{min}(L(\mathbf{r}^k))} + \frac{1}{\sigma_{min}(L_S(\mathbf{r}^k))} \leq \frac{2}{\sigma_{min}(L(\mathbf{r}^k))} \\ &\leq \frac{2}{\min_{1 \leq k \leq n} \sigma_{min}(L(\mathbf{r}^k))} \end{aligned}$$

and the claim follows.

Proof of Proposition 3.5

From (2.21) and Proposition 3.1 we get

$$\begin{aligned} \|\widetilde{Q}_{wMNE}\| &= \|\widetilde{G}_{wMNE}^{-1} M_S^T b\| \leq \|\widetilde{G}_{wMNE}^{-1}\| \|M_S^T b\| \\ &\leq \frac{1}{\mu} \|M_S^T b\| \leq \frac{1}{\mu} \|M^T b\|. \end{aligned}$$

The last inequality is a consequence of the fact that $M_S^T b \in \mathbb{R}^c$ while $M^T b \in \mathbb{R}^n$.
The inequality for $\|Q_{wMNE}\|$ can be proved in a similar way.

Bibliography

[1] Sylvain Baillet, John C Mosher, and Richard M Leahy. Electromagnetic brain mapping. *IEEE Signal Processing Magazine*, 18(6):14–30, 2001.

[2] Roberta Grech, Tracey Cassar, Joseph Muscat, Kenneth P Camilleri, Simon G Fabri, Michalis Zervakis, Petros Xanthopoulos, Vangelis Sakkalis, and Bart Vanrumste. Review on solving the inverse problem in EEG source analysis. *Journal of Neuroengineering and Rehabilitation*, 5(1):1–33, 2008.

[3] Daniela Calvetti, Harri Hakula, Sampsa Pursiainen, and Erkki Somersalo. Conditionally Gaussian hypermodels for cerebral source localization. *SIAM Journal on Imaging Sciences*, 2(3):879–909, 2009.

[4] Stefan Haufe, Sven Dähne, and Vadim V Nikulin. Dimensionality reduction for the analysis of brain oscillations. *Neuroimage*, 101:583–597, 2014.

[5] Axel Faes, Aurélie de Borman, and Marc Van Hulle. Source space reduction for eLORETA. *Journal of Neural Engineering*, 18(6):066014, 2021.

[6] Francesca Pitolli and Cristina Pocci. Neuroelectric source localization by random spatial sampling. *Journal of Computational and Applied Mathematics*, 296:237–246, 2016.

[7] Matti Hämäläinen, Riitta Hari, Risto J Ilmoniemi, Jukka Knuutila, and Olli V Lounasmaa. Magnetoencephalography: theory, instrumentation and applications to non-invasive studies of the working human brain. *Reviews of Modern Physics*, 65:413–498, 1993.

[8] Annalisa Pascarella and Francesca Pitolli. An inversion method based on random sampling for real-time MEG neuroimaging. *Communications in Applied and Industrial Mathematics*, 10(2):25–34, 2019.

[9] Cristina Campi, Annalisa Pascarella, and Francesca Pitolli. Less is enough: Assessment of the random sampling method for the analysis of magnetoencephalography (MEG) data. *Mathematical and Computational Applications*, 24(4):98, 2019.

[10] Matti Hämäläinen and Risto J Ilmoniemi. Interpreting magnetic fields of the brain: minimum norm estimates. *Medical & Biological Engineering & Computing*, 32:35–42, 1994.

[11] Roberto Domingo Pascual-Marqui. Standardized low-resolution brain electromagnetic tomography (sLORETA): technical details. *Methods & Findings in Experimental & Clinical Pharmacology*, 24(Suppl D):5–12, 2002.

[12] Kenneth L Clarkson. Subgradient and sampling algorithms for ℓ_1 regression. In *Symposium on Discrete Algorithms: Proceedings of the Sixteenth Annual ACM-SIAM Symposium on Discrete algorithms*, volume 23, pages 257–266, 2005.

[13] Vladimir Rokhlin and Mark Tygert. A fast randomized algorithm for overdetermined linear least-squares regression. *Proceedings of the National Academy of Sciences*, 105(36):13212–13217, 2008.

[14] Haim Avron, Kenneth L Clarkson, and David P Woodruff. Faster kernel ridge regression using sketching and preconditioning. *SIAM Journal on Matrix Analysis and Applications*, 38(4):1116–1138, 2017.

[15] Petros Drineas and Michael W Mahoney. Lectures on randomized numerical linear algebra. *The Mathematics of Data*, 25(1), 2018.

[16] Nathan Halko, Per-Gunnar Martinsson, and Joel A Tropp. Finding structure with randomness: Probabilistic algorithms for constructing approximate matrix decompositions. *SIAM Review*, 53(2):217–288, 2011.

[17] Hua Xiang and Jun Zou. Regularization with randomized SVD for large-scale discrete inverse problems. *Inverse Problems*, 29(8):085008, 2013.

[18] Hua Xiang and Jun Zou. Randomized algorithms for large-scale inverse problems with general Tikhonov regularizations. *Inverse Problems*, 31(8):085008, 2015.

[19] Yimin Wei, Pengpeng Xie, and Liping Zhang. Tikhonov regularization and randomized GSVD. *SIAM Journal on Matrix Analysis and Applications*, 37(2):649–675, 2016.

[20] Kazufumi Ito and Bangti Jin. Regularized linear inversion with randomized singular value decomposition. In L Beilina and et al, editors, *Mathematical and Numerical Approaches for Multi-wave Inverse Problems*, pages 45–72. Springer, 2019.

[21] Shuai Lu, Peter Mathé, and Sergei V Pereverzev. Randomized matrix approximation to enhance regularized projection schemes in inverse problems. *Inverse Problems*, 36(8):085013, 2020.

[22] J Tanner Slagel, Julianne Chung, Matthias Chung, David Kozak, and Luis Tenorio. Sampled Tikhonov regularization for large linear inverse problems. *Inverse Problems*, 35(11):114008, 2019.

[23] Atena Rezaei, Alexandra Koulouri, and Sampsa Pursiainen. Randomized multiresolution scanning in focal and fast E/MEG sensing of brain activity with a variable depth. *Brain Topography*, 33(2):161–175, 2020.

[24] Atena Rezaei, Joonas Lahtinen, Frank Neugebauer, Marios Antonakakis, Maria Carla Piastra, Alexandra Koulouri, Carsten H Wolters, and Sampsa Pursiainen. Reconstructing subcortical and cortical somatosensory activity via the RAMUS inverse source analysis technique using median nerve sep data. *Neuroimage*, 245:118726, 2021.

[25] Petros Drineas, Ravi Kannan, and Michael W Mahoney. Fast Monte Carlo algorithms for matrices I: Approximating matrix multiplication. *SIAM Journal on Computing*, 36(1):132–157, 2006.

[26] Georg Northoff. *Unlocking the brain. Volume 1: Coding*. Oxford University Press, 2014.

[27] Rajendra Bhatia. *Perturbation bounds for matrix eigenvalues*. SIAM, 2007.

[28] Gene H Golub and Charles F Van Loan. *Matrix computations*. JHU press, 2013.

[29] Fa-Hsuan Lin, Thomas Witzel, Seppo P Ahlfors, Steven M Stufflebeam, John W Belliveau, and Matti S Hämäläinen. Assesing and improving the spatial accuracy in MEG source localization by depth-weighted minimun norm estimates. *Neuroimage*, 31:160–171, 2006.

[30] Fa-Hsuan Lin, John W Belliveau, Anders M Dale, and Matti S Hämäläinen. Distributed current estimates using cortical orientation constraints. *Human Brain Mapping*, 27:1–13, 2006.

[31] Annalisa Pascarella and Alberto Sorrentino. Statistical approaches to the inverse problem. In Pang Elizabeth, editor, *Magnetoencephalography*, pages 93–112. InTech, Rijeka, Croatia, 2011.

[32] Alexandre Gramfort, Théodore Papadopoulo, Emmanuel Olivi, and Maureen Clerc. OpenMEEG: opensource software for quasistatic bioelectromagnetics. *Biomedical Engineering Online*, 9:1–20, 2010.

[33] Bruce Fischl, Martin I Sereno, Roger BH Tootell, and Anders M Dale. High-resolution intersubject averaging and a coordinate system for the cortical surface. *Human Brain Mapping*, 8(4):272–284, 1999.

[34] François Tadel, Sylvain Baillet, John C Mosher, Dimitrios Pantazis, and Richard M Leahy. Brainstorm: a user-friendly application for MEG/EEG analysis. *Computational Intelligence and Neuroscience*, 2011:1–13, 2011.

[35] Olaf Hauk, Daniel G Wakeman, and Richard Henson. Comparison of noise-normalized minimum norm estimates for MEG analysis using multiple resolution metrics. *Neuroimage*, 54(3):1966–1974, 2011.

[36] Nicholas Metropolis and Stanislaw Ulam. The Monte Carlo method. *Journal of the American Statistical Association*, 44(247):335–341, 1949.

[37] Alan Frieze, Ravi Kannan, and Santosh Vempala. Fast Monte-Carlo algorithms for finding low-rank approximations. In *Proceedings of 39th Symposium on Foundations of Computer Science*, pages 370–378. IEEE Computer Society Press, Los Alamitos, Calif., 1998.

[38] Alan Frieze, Ravi Kannan, and Santosh Vempala. Fast Monte-Carlo algorithms for finding low-rank approximations. *Journal of the ACM*, 51(6):1025–1041, 2004.

[39] Sara Sommariva and Alberto Sorrentino. Sequential Monte Carlo samplers for semi-linear inverse problems and application to magnetoencephalography. *Inverse Problems*, 30:114020, 2014.

[40] Massimo Fornasier and Francesca Pitolli. Adaptive iterative thresholding algorithms for magnetoencephalography (MEG). *Journal of Computational and Applied Mathematics*, 221(2):386–395, 2008.

[41] Stefan Haufe, Vadim Nikulin, Andreas Ziehe, Klaus-Robert Müller, and Guido Nolte. Estimating vector fields using sparse basis field expansions. In D Koller and et al, editors, *NIPS'08: Proceedings of the 21st International Conference on Neural Information Processing Systems*, pages 617–624, 2008.

[42] Petros Drineas, Ravi Kannan, and Michael W Mahoney. Fast Monte Carlo algorithms for matrices II: Computing a low-rank approximation to a matrix. *SIAM Journal on Computing*, 36(1):158–183, 2006.

[43] Younes Sadat-Nejad and Soosan Beheshti. Efficient high resolution sLORETA in brain source localization. *Journal of Neural Engineering*, 18(1):016013, 2021.

[44] Pavitra Krishnaswamy, Gabriel Obregon-Henao, Jyrki Ahveninen, Sheraz Khan, Behtash Babadi, Juan Eugenio Iglesias, Matti S Hämäläinen, and Patrick L Purdon. Sparsity enables estimation

of both subcortical and cortical activity from MEG and EEG. *Proceedings of the National Academy of Sciences*, 114(48):E10465–E10474, 2017.